An Experimental and Analytical Study of the Large Strain Response of Glassy Polymers with a Noncontact Laser Extensometer

G. SPATHIS, E. KONTOU

Department of Engineering Science, Section of Mechanics, National Technical University of Athens, 5 Heroes of Polytechnion, GR-15773, Athens, Greece

Received 13 March 1998; accepted 5 August 1998

ABSTRACT: The yield behavior of an amorphous glassy polymer has been studied with true tensile stress–strain curves, obtained at various crosshead speeds by means of a new experimental method. A constitutive equation from nonlinear viscoelasticity has been used, with the further assumption that the material, during deformation, subsequently follows the following two distinct paths: a nonlinear viscoelastic, and a plastic one. The maximum strain, where this distinction is manifested, has been treated as a control parameter, while the strain rate was experimentally evaluated. The decomposition of deformation has been made with a suitable kinematic formulation, proposed in the literature. The theoretical results describe the experimental curves in detail. © 1999 John Wiley & Sons, Inc. J Appl Polym Sci 71: 2007–2015, 1999

Key words: yield behavior; stress–strain response; deformation; glassy polymers; noncontact measurement

INTRODUCTION

Glassy polymers constitute a large class of engineering materials so that it is interesting to quantify the large inelastic deformation behavior of these materials. Such behavior is known to exhibit strain rate, temperature, and a pressure-dependent yield, as well as true strain softening and strain hardening after yield.

In the description of the deformation behavior of solid polymers, a distinction is usually made between the linear viscoelastic regime at low strain, the nonlinear viscoelastic response at moderate strain, and the yield behavior at high strain values, as has been mentioned elsewhere.[1,2]

The linear viscoelastic deformation is adequately described using the linear response theory, while the nonlinear regime is still a field of research. On the other hand, the yield of polymeric materials is classically described by using yield criteria, with the pressure- and rate-dependent von Mises criterion being more successful. Several attempts have been made to describe the large deformation of glassy polymers, by Boyce et al.,[3] or by Wu and van der Giessen,[4] that combine the elastoviscoplastic response at small strains and the strain hardening effect after yield.

Another approach assumes that yielding in polymers is related to a molecular relaxation process, occurring when the plastic flow rate is equal to the applied strain rate. The use of a stress-dependent relaxation time was initially introduced by Tobolsky and Eyring.[5] It was modified later by Haward and Thackray,[6] who proposed a Langevin spring to account for the finite extensibility of the entanglement network. However, the use of a single relaxation time cannot account for the viscoelastic response at small and moderate

Correspondence to: G. Spathis.

Journal of Applied Polymer Science, Vol. 71, 2007–2015 (1999)
 CCC 0021-8995/99/122007-09

strains. Therefore, a spectrum of relaxation times would be more appropriate. If it is further assumed that the relaxation times depend on the same way on the total stress, the principle of time–stress superposition has been applied by Bernstein and Shokooh,[7] which is equivalent to the time–temperature superposition.

In this work, a constitutive model is developed that combines the initial viscoelastic deformation behavior of polymeric glasses, at small and moderate strains, with the post-yield plastic flow, accompanied by a strain softening and strain hardening.

The following analysis is based on the idea that there are two distinct paths, followed by the material during the deformation procedure. In the first stage, at small strains, the viscoelastic path is dominant, and the corresponding constitutive relations, according to the nonlinear viscoelastic description by Matsuoka,[8] are expressed as the product of a strain-dependent term with a time-dependent one. This behavior is extended up to a critical value of deformation, which acts as a control parameter of the whole behavior of the material. At this point, a localized domain breakage takes place inside the structure of the material, according to Matsuoka's treatment, revealing a totally new behavior this way. Hereafter, the plastic path prevails.

For a suitable application of the above constitutive equation, a kinematic description is necessary to separate from the total deformation the part, which will be used in the viscoelastic response, and the other one, which follows the plastic flow behavior. This kinematic formulation is based on an earlier work developed by Rubin[9] and used by Spathis and Kontou.[10] According to this treatment, an evolution equation for the first type of deformation has been defined, without specifying a plastic deformation tensor explicitly.

Moreover, in the following treatment, the exact knowledge of the rate of deformation, as well as the characteristic strain value, at which the phenomenon of the separation of the two paths is disclosed, is very significant. The intrinsic plastic behavior of ductile materials has been extensively studied by G'Sell et al.[11] They developed a novel technique that analyzes the sample profile in real time, while the effective strain is recorded from the minimum specimen diameter. Moreover, with an appropriate control system, the local effective strain rate is maintained constant.

In our study, the strain rate and the final elastic strain value, have been determined experimentally, by a new device. This system allows a noncontact measurement of longitudinal deformation on the sample, while the load is recorded simultaneously. For a constant crosshead speed experiment, it was found that the local strain rate appears to vary by one or two orders of magnitude across the specimen gauge length. The time evolution of local strain and local strain rate could be recorded and introduced into the constitutive model. Moreover, the tensile stress had to be corrected for this strain variation with the further assumption that the deformation procedure is isochoric. Then the true stress–strain curves have been constructed for tensile experiments at four different crosshead speeds tested. The theoretical description of experimental results has then been made successfully, while the parameters used are grounded on a physical base.

MATERIALS AND EXPERIMENTAL

The material tested was polycarbonate, with the commercial name Lexan, provided in plate form. Dogbone tensile specimens have then been constructed with an average thickness of 2 mm, an average width of 3.8 mm, and a gauge length of 30 mm. In order to eliminate any prehistory effects, the samples were annealed at a temperature above T_g for 1 h. The tensile experiments have been carried out with an Instron 1121 tester at room temperature. Four different crosshead speeds have been used, namely, 0.1, 1, 5, and 10 mm/min. The longitudinal strain could be measured very accurately, with the laser extensometer, which permits a noncontact measurement of the longitudinal deformation distribution of samples. This experimental method is presented in detail in Spathis and Kontou.[10]

For the elongation measurements, a high-contrast tape pattern code was applied to the gauge length of the sample, namely, 15 white stripes on dark background. The space between stripes was 1 mm.

During the tensile tests, the load was recorded simultaneously with the percentage strain, and the data acquisition has been made with a software. The construction of engineering and true stress–strain curves was then made, as will be discussed below.

EXPERIMENTAL RESULTS

In this study, a noncontact method of deformation measurement has been used. This technique per-

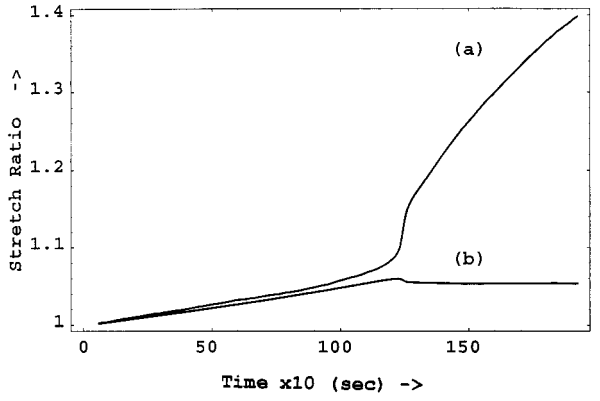

Figure 1 (a) Strain variation versus time for the zone with maximum deformation and (b) a representative zone that deforms elastically for the crosshead speed of 0.1 mm min.

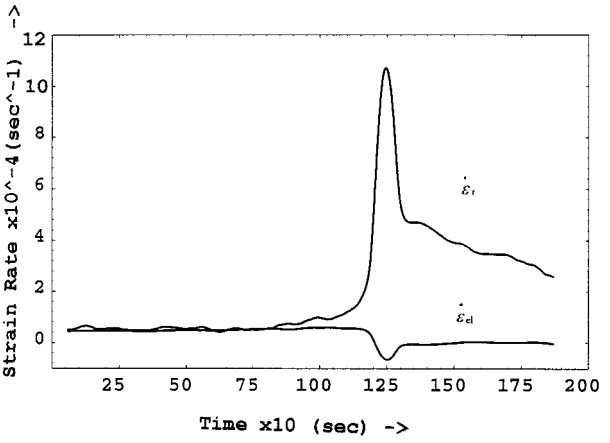

Figure 2 Strain rate variation versus time with respect to Figure 1. Curve $\dot{\varepsilon}_r$ corresponds to the data of Figure 1(a), and $\dot{\varepsilon}_{el}$ corresponds to the data of Figure 1(b).

mits the detailed description of the deformation distribution along the gauge length, in every zone separately. In the case of nonuniform deformation, where necking initiation and neck propagation takes place, the specific zone where these effects are exhibited can be specified. The time evolution of strain along the zone with maximum deformation is presented in Figure 1 as curve (a), as well as a representative plot for the corresponding strain along the zones, that are deformed elastically, namely, curve (b). As is observed, during the initial elastic response, all zones have almost the same strain. When plastic instability emerges, followed by necking initiation, a large deviation of strain appears, as shown in curve (a), compared to the rest of the regions [curve (b)] Fig. 1, that are still deforming elastically. These zones appear to have a decremental trend at the same time. This behavior takes place in a very short time interval; hereafter, the slope of strain increment in curve (a) decreases due to the fact that neck propagates and extends through the entire zone.

This picture may be clearly presented in terms of strain rate versus time in Figure 2. In this figure, curve of $\dot{\varepsilon}_r$ represents the strain rate varying with time for the zone with maximum deformation, while curve, defined as $\dot{\varepsilon}_{el}$, shows the strain rate dependence of a representative zone that deforms elastically. Here, the sudden increase of strain rate $\dot{\varepsilon}_r$ is more obvious, extended in a very short time, while this effect is less profound for the other zone.

If the data of Figure 2 are plotted with respect to stretch ratio, as shown in Figure 3, the exact value of strain where plastic instability takes place can be defined. From this picture, we observe that, initially, the strain rate is very slow and almost equal to the imposed strain rate. Then $\dot{\varepsilon}_r$ speeds up, reaching a high value, and remains constant as long as neck propagation continues. When necking exceeds the boundaries of this zone, a decrement of strain rate appears, exhibiting the initiation of strain hardening. At this stage, the stretch ratio at which this effect takes place can be accurately defined.

In Figure 4, strain rate versus strain for the four different crosshead speeds examined is presented. In all cases, the data correspond to the zone with maximum deformation. The shape of this plot remains constant, while the values are

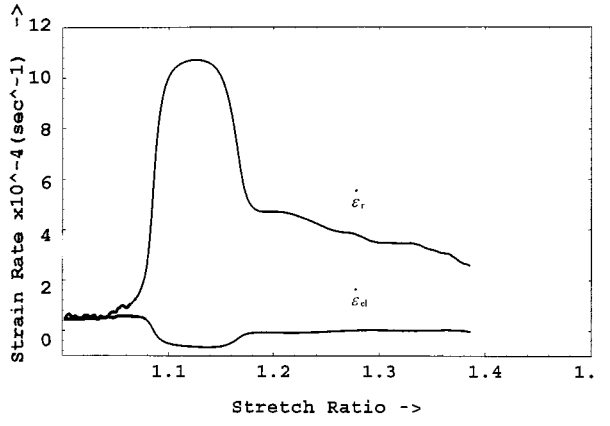

Figure 3 The experimental results of Figure 2 with respect to the stretch ratio.

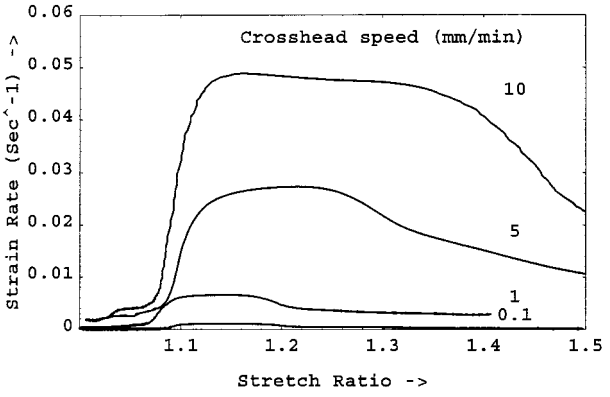

Figure 4 Strain rate of zone with maximum elongation with respect to the stretch ratio for four different crosshead speeds tested.

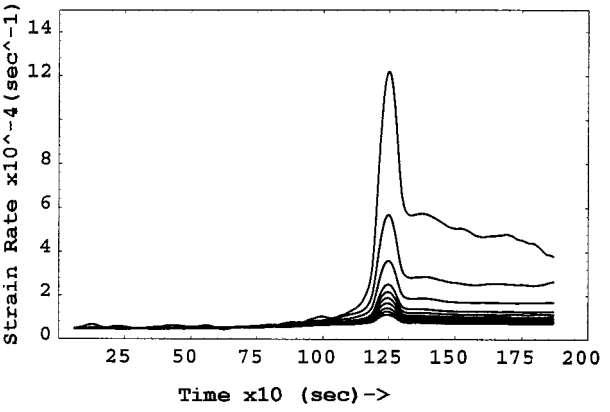

Figure 5 Strain rate versus time of regions, including an increasing number of successive zones, starting from the reference one.

scaled in respect to the crosshead speeds tested. Moreover, an interesting remark can be made regarding this plot. The onset of yielding, which is accompanied by the rapid increase of strain rate, is exhibited in a narrow region of strain, for all crosshead speeds tested, and this value is approximately equal to 0.04. This value represents the maximum elastic strain, is material-dependent, and for glassy polymers has a value close to 0.1, as is also reported by Matsuoka.[8]

It is assumed here that all glassy polymers are characterized by such a universal parameter that controls the initiation of plastic behavior and is slightly strain-rate-dependent, as compared to the strong rate dependence of the yield stress. In the following analysis, it will be considered that this parameter controls the transition from elastic to plastic behavior.

If we had the possibility to reduce the length of the zone with neck initiation, to the dimension of the localized region, where the onset of yielding takes place, then the respective strain rate would be equal to the plastic rate of deformation. In order to approximate this value, a scaling procedure has been followed. In Figure 5, plots of strain rates of various reference lengths, starting from the one with the neck initiation and moving equivalently from both sides up to the total specimen gauge length, are presented for a crosshead speed equal to 0.1 mm/min.

As is observed from this figure, the corresponding strain rate plots are scaled into similar forms, taking even lower values. Assuming that the same scaling form will be retained if we move to smaller gauge lengths towards the microscopic plastic zone, we can conclude that the rate of plastic deformation Γ_p is

$$\Gamma_p = k(\dot{\varepsilon}_r - \dot{\varepsilon}_{\mathrm{el}}) \tag{1}$$

where k is an amplification factor, which will be defined below, and $\dot{\varepsilon}_r$ and $\dot{\varepsilon}_{\mathrm{el}}$ are the strain rate of the zone with maximum deformation and of the zone deforming elastically, respectively. These two magnitudes are also plotted in Figure 2.

The load deformation data for all crosshead speeds tested are presented in Figure 6, in terms of engineering stress. However, due to the inhomogeneous deformation of the material, exhibited initially by neck formation and followed by a subsequent neck propagation along the specimen gauge length, this conventional determination of tensile data does not adequately describe the intrinsic behavior of the material. Therefore, the experimental data have been replotted in terms of

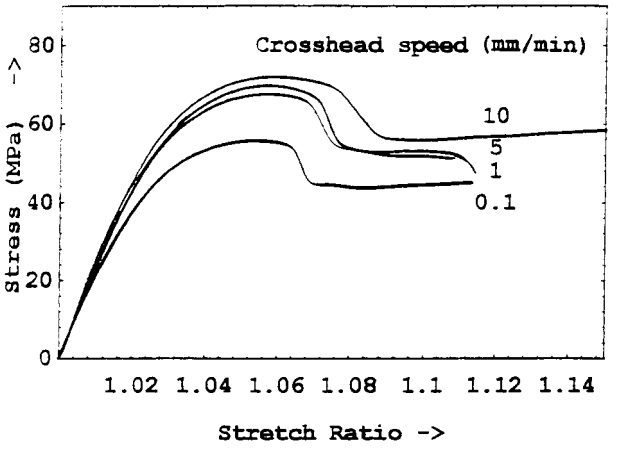

Figure 6 Engineering tensile stress–strain plots of polycarbonate at four different crosshead speeds.

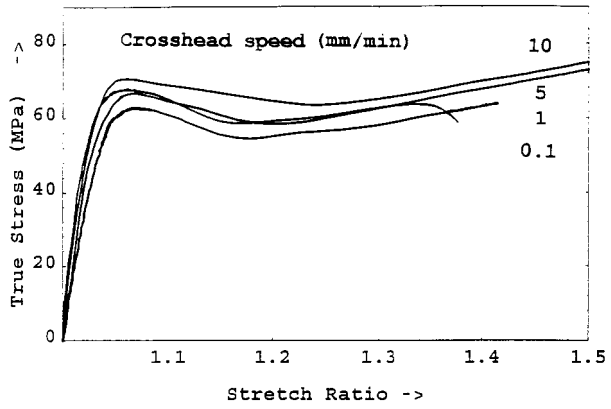

Figure 7 True tensile stress–strain plots of polycarbonate at four different crosshead speeds with respect to the zone with maximum elongation.

true stress–strain curves, in Figure 7, assuming an isochoric deformation procedure. More specifically, the true stress and true strain have been defined in local terms, as follows:

$$\sigma = \frac{P}{A} = \left(\frac{P}{A_0}\right)\left(\frac{l}{l_0}\right)$$

$$\varepsilon = \lim_{l_0 \to 0}\left[\ln\left(\frac{l}{l_0}\right)\right] \tag{2}$$

where A and A_0 are the current and initial areas of cross section, respectively, and length l_0 and l are the initial and current length of a small slice of the specimen located at the point where σ and ε are defined. In our case, this small slice of the sample is the zone of 1 mm, where the neck initiation occurs. The possible curvature that may occur with neck formation is assumed to have negligible contribution on the calculation of stress because the radius of this curvature is very large compared to the dimensions of the cross section. Moreover, as neck propagates, the reference zone where the deformation measurement, if focused, remains prismatic. Therefore, if the same procedure to that by G'Sell et al.[11] is followed, where the effective stress is scaled with the triaxiality factor F_T, introduced for the necking phenomena by Bridgman,[12] it may be extracted that this factor has a negligible effect, for the geometry of the samples tested.

From both figures, the rate dependence of yield stress is obvious while the yield strain or the final elastic strain seems to be slightly strain-rate-sensitive. Therefore, this value is assumed to be constant and almost equal to 0.04, as mentioned above.

The initial slope of the stress–strain plot up to yield stress exhibits a varied curvature, which is commonly abounded in viscoelastic materials, when constant strain rate experiments are executed. The rate dependence of the yield stress and the shape of these plots up to yield initiation lead to the conclusion that this behavior is not purely elastic, exhibiting viscoelastic features, and is described with the following analysis.

CONSTITUTIVE EQUATIONS FOR UNIAXIAL STRESS

The first stage of deformation procedure will be described through a viscoelastic path, which is controlled by a spectrum of relaxation times, as in the analogy, is proposed in Tervoort et al.[1] The maximum stress corresponds to the terminal value that is obtained when the material region with the highest relaxation time breaks down.[8] This occurrence takes place at a certain strain,

$$\dot{\varepsilon}\lambda = \bar{\varepsilon} \tag{3}$$

where $\dot{\varepsilon}$ is the imposed strain rate, and λ is the relaxation time. In our case, $\bar{\varepsilon}$ is equal to 0.04, as discussed above.

Following as a possible mechanism, the viscoelastic path, the formulation of stress may be given by the following expression, which is also used in Matsuoka.[8]

$$\sigma = \mathrm{E}_0\bar{\varepsilon}\left[1 - \exp\left[-\frac{\varepsilon}{\bar{\varepsilon}}\right]\right] \tag{4}$$

From the above treatment, it may be concluded that the magnitude of $\bar{\varepsilon}$ is a crucial factor that determines whether the viscoelastic or plastic path is followed, as proposed in Matsuoka.[8] After the critical strain $\bar{\varepsilon}$ is reached and the terminal stress is obtained, the material follows a plastic path already existing in a latent condition up to this stage; hereafter, it manifests, followed by a subsequent breakage of material domains. At this stage, a set of constitutive equations should be necessary to describe the plastic flow. A suitable kinematic formulation will be used for separating the total deformation in the following two parts: the plastic one that follows an associate flow rule, and the remaining part that is related with

the viscoelastic constitutive equation, mentioned above. This decomposition has been made following previous works by Rubin.[9]

Although Rubin's treatment has been introduced for describing a general anisotropic response of crystalline metals, his analysis can be applied as a constitutive theory for the general description of plastic behavior of materials.

According to his assumption, the elastic deformation of each material point has been formulated through a triad of vectors $\boldsymbol{m_i}$, that are related to dilatation, distortion, and orientation of a mean atomic lattice in respect to some reference state. To avoid the decomposition of the deformation gradient tensor into elastic and plastic parts, because these tensors lack an explicit determination in the present configuration of the material elements, Rubin specified an evolution equation for the elastic deformation, including the relaxation effect of plastic deformation, without introducing a plastic deformation tensor explicitly. It is assumed here that the triad of vectors $\boldsymbol{m_i}$ is defined to characterize the deformation state of a material element, and they constitute a set of orthonormal vectors, implying that the corresponding metric tensor m_{ij} equal to $m_{ij} = \boldsymbol{m_i} \cdot \boldsymbol{m_j}$ is given by

$$m_{ij} = \delta_{ij} \tag{5}$$

In order to define the change of the volume element we are referred to, the dilatation J_m (which is unity in the reference state) is introduced and given by

$$J_m = \boldsymbol{m}_1 x(\boldsymbol{m}_2 \cdot \boldsymbol{m}_3) = (detm_{ij})^{1/2} \tag{6}$$

Moreover, to define the distortional measures of the elementary volume, Rubin has introduced another set of orthonormal vectors $\boldsymbol{m_i'}$ defined by the following equations:

$$\boldsymbol{m_i'} = J_m^{-1/3}\boldsymbol{m_i} \quad \text{with} \quad m_{ij}' = \boldsymbol{m_i'} \cdot \boldsymbol{m_j'} = J_m^{-2/3} m_{ij} \tag{7}$$

It is easily then extracted that

$$detm_{ij}' = 1 \tag{8}$$

The microstructural variables m_i are determined by an evolution equation of the following form:

$$\dot{\boldsymbol{m}}_i = \boldsymbol{L}_m \boldsymbol{m}_i \tag{9}$$

where the second-order tensor $\boldsymbol{L_m}$ corresponds to the elastic velocity gradient and is assumed to be separated additively into the form:

$$\boldsymbol{L}_m = \boldsymbol{L} - \boldsymbol{L}_p \tag{10}$$

where $\boldsymbol{L}$ and $\boldsymbol{L}_p$ are the velocity gradients of total and plastic deformation, respectively.

Concerning uniaxial stress in the $\boldsymbol{e_1}$ direction in respect to a fixed rectangular Cartesian base vector $\boldsymbol{e}_i$ parallel to $\boldsymbol{m}_i$, it can be shown that the velocity gradient is specified by the following form:

$$\boldsymbol{L} = \boldsymbol{D} = \frac{\dot{a}}{a}\boldsymbol{e}_1 \otimes \boldsymbol{e}_1 + \frac{\dot{b}}{b}\boldsymbol{e}_2 \otimes \boldsymbol{e}_2 + \frac{\dot{c}}{c}\boldsymbol{e}_3 \otimes \boldsymbol{e}_3 \tag{11}$$

where the symbol $\otimes$ denotes the tensor product between two vectors, and a, b, and c represent the stretches of material line elements in the coordinate directions $\boldsymbol{e_1}$, $\boldsymbol{e_2}$ and $\boldsymbol{e_3}$, respectively, with following initial conditions:

$$a(0) = b(0) = c(0) = 1 \tag{12}$$

The antisymmetric part $\boldsymbol{W}$ of the velocity gradient and consequently $\boldsymbol{W}_p$ vanish in the case of uniaxial stress, resulting in

$$\boldsymbol{L}_p = \boldsymbol{D}_p \tag{13}$$

Then, the corresponding constituents of the distortional vector $\boldsymbol{m_i'}$ may be represented by the following forms.

$$m_{33}' = a_m^2, \quad m_{11}' = m_{22}' = \frac{1}{a_m}$$

$$\boldsymbol{m}_3' = a_m \boldsymbol{e}_3,$$

$$\boldsymbol{m}_1' = \frac{1}{\sqrt{a_m}}\boldsymbol{e}_1, \; \boldsymbol{m}_2' = \frac{1}{\sqrt{a_m}}\boldsymbol{e}_2 \tag{14}$$

where a_m is a function to be determined.

The deviatoric part $\boldsymbol{D'}$ of $\boldsymbol{D}$ may be defined by the following equation:

$$\boldsymbol{D'} = \boldsymbol{D} - \tfrac{1}{3}(\boldsymbol{D} \cdot \boldsymbol{I})\boldsymbol{I} \tag{15}$$

Combining equations (6), (7), (9), and (10) gives

$$\frac{\dot{J}_m}{J_m} = tr\boldsymbol{L}_m = \boldsymbol{D}\cdot\boldsymbol{I}$$

$$\dot{m}'_{ij} = 2(\boldsymbol{D} - \boldsymbol{D}_p)\cdot(\boldsymbol{m}'_i \otimes \boldsymbol{m}'_j) \tag{16}$$

where the dot product $\boldsymbol{A}\cdot\boldsymbol{B}$ between two tensors denotes the usual scalar product when $\boldsymbol{A}$ and $\boldsymbol{B}$ are vectors, and it denotes the scalar $\mathrm{tr}(\boldsymbol{AB}^T)$ when $\boldsymbol{A}$ and $\boldsymbol{B}$ are second-order tensors.

The associate flow rule, which defines the symmetric part of the plastic velocity gradient D_p, has been written by Rubin as

$$\boldsymbol{D}_p = \Gamma_p \bar{\boldsymbol{D}}_p \tag{17}$$

where the direction of $\bar{\boldsymbol{D}}_p$ for a plastically isotropic response is specified by the deviatoric portion of the driving stress tensor, and Γ_p is a nonnegative function expressing the rate of plastic deformation and needs to be specified.

For the case of uniaxial deformation, Rubin, solving the above equations, extracted the following expression for the time evolution of the stretch ratio a_m, of the volume element, which is subjected to the large imposed deformation.

$$\frac{\dot{a}_m}{a_m} = \left[\frac{1 + \dfrac{1-2v}{2(1+v)}\left(\dfrac{a_m^3 - 1}{a_m}\right)}{1 + \dfrac{1-2v}{6(1+v)}\left(\dfrac{5a_m^3 - 2}{a_m}\right)}\right] \times \left[\frac{\dot{a}}{a} - \frac{\Gamma_p}{18}\left(\frac{a_m^3 - 1}{a_m^3}\right)(4\,a_m^3 + 2)\right] \tag{18}$$

with the initial condition $a_m(0) = 1$, and v is the Poisson ratio.

The functional form of Γ_p has been mentioned in the previous section and expressed by eq. (1). The amplification factor k of eq. (1) is considered to be strain-rate-independent and state-of-deformation-independent. Consequently, k can be evaluated at the stage where yield initiates, and the stretch ratio a_m is approximately equal to 1, while $\dot{a}_m$ is almost equal to zero. Then the second term of the second part of eq. (18) is equal to zero. Using the above approximations, we obtain

$$\Gamma_p \cong \frac{\dot{a}}{a}\frac{1}{a_m - 1} \tag{19}$$

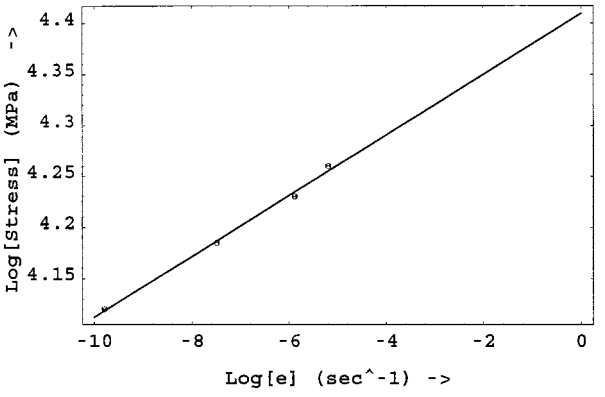

Figure 8 Yield stress versus strain rate plotted logarithmically at four different strain rates examined.

At the reference zone, $\dot{a}$ is equal to $\dot{\varepsilon}_r$, and the coefficient k is equal to $1/a(a_m - 1)$ or equal to $1/a\bar{\varepsilon}$, where $\bar{\varepsilon}$ is the terminal elastic strain of this zone, and $a \cong 1.0$, as is shown in the experimental data of Figure 7. At the yield point, $\bar{\varepsilon}$ is considered to be constant equal to 0.04, and, consequently, k is equal to 25.

The integration of eq. (18) determines the value of stretch ratio $\dot{a}_m$ at every state of elongation. By incorporating the corresponding magnitude of strain into the viscoelastic constitutive eq. (4), the calculation of stress can be made.

The integration method has been made numerically, using small time steps, with the software *Mathematica* developed by Wolfram[13] and a personal computer. Gradually decreasing the original time step up to one-tenth, a high convergence has been obtained.

In order to describe the material response at various crosshead speeds, a scaling rule, widely applied in the viscoplasticity by Matsuoka,[8] has been used. Following this rule, a stress–strain curve at a strain rate $\dot{\varepsilon}_2$ can be predicted from an experimental curve obtained at a rate $\dot{\varepsilon}_1$ by multiplying the stress in the experimental curve by the scaling factor $(\dot{\varepsilon}_2/\dot{\varepsilon}_1)$,^{n} where $\dot{\varepsilon}_2$ represents the imposed strain rate of 10 mm/min and $\dot{\varepsilon}_1$ corresponds to the speed of 0.1 mm/min. Both values of these strain rates are taken to be constant, equal to the average value of the imposed crosshead speed reduced to the total specimen gauge length. Following this scaling law, the data of the intermediate speeds can also be extracted.

The calculation of the exponent n can be made in terms of the slope of the variation of the yield stress plotted logarithmically with respect to strain rate. Following Figure 8, where experimen-

tal yield stress is presented versus strain rate, exponent n has been found equal to 0.028.

As has been testified in the experimental results of the stress–strain curves, a strain hardening takes place in a specific value of the stretch ratio. This specific stretch ratio can also be defined from the variation of strain rate versus strain, where a great decrement of strain rate magnitude is observed. At this point, the plastic deformation has been spread throughout the reference zone; hereafter, every molecular alignment results to a strain hardening. To obtain the complete calculation of the stress, including this stage of deformation, a supplementary term for stress should be taken into account due to the entropic hardening.

The entropic hardening term can be represented as a stress based on the theory of rubber elasticity of Kuhn and Grun.[14] The modelling of entropic resistance has also been reported by Parks et al.[15] Upon stretching, the chains begin to orient in an affine manner, and this effect can be described by the statistical mechanics network models of rubber elasticity. In our case, the three-chain model of James and Guth[16] has been used. In this way, the total stress may be expressed as

$$\begin{aligned} \sigma_{\text{total}} &= \sigma \qquad \text{for } a \le a^* \\ \sigma_{\text{total}} &= \sigma + \sigma_h \quad \text{for } a \ge a^* \end{aligned} \tag{20}$$

where σ is obtained by solving the system of equations (1), (4), (18), and (19), a^* is the stretch ratio of the onset of strain hardening, and σ_h is a stress attributed to the strain hardening and is given by

$$\sigma_h = G_p \frac{\sqrt{N}}{3}\left[\lambda_i L^{-1}\left(\frac{\lambda_i}{\sqrt{N}}\right) - \frac{1}{3}\sum_{j=1}^{3}\lambda_j L^{-1}\left(\frac{\lambda_j}{\sqrt{N}}\right)\right] \tag{21}$$

where λ_i are the stretch ratios in the three principal directions, with $\lambda_1 = a$ and $\lambda_2 = \lambda_3 = 1/a\wedge.5$. N is the equivalent number of rigid links between entanglements. As is mentioned by Boyce et al.,[3] $\sqrt{N}$ is equal to the terminal or locking stretch. From the true stress–strain curves of Figure 7, it is shown that locking occurs at a strain almost equal to 0.5, resulting in a value for N approximately equal to 3. G_p is the strain hardening modulus taken to be equal to 18 MPa.

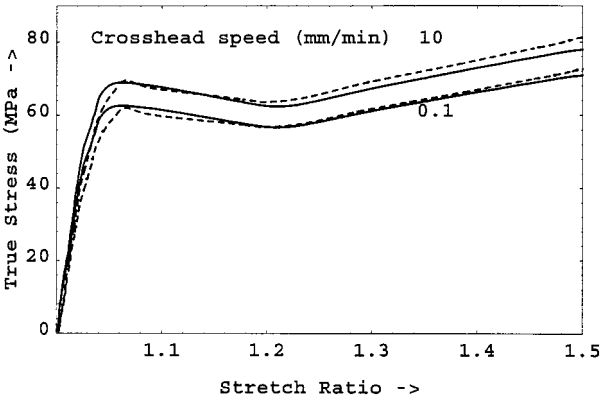

Figure 9 True tensile stress–strain plots of polycarbonate at two crosshead speeds. Dashed lines represent theoretical results; solid lines represent experimental results.

The theoretical results of stress versus strain are plotted in respect to the experimental ones, in Figure 9, at two different crosshead speeds, namely, 0.1 and 10 mm/min.

CONCLUSIONS

In this work, the intrinsic tensile stress–strain response of polycarbonate at various crosshead speeds has been evaluated by means of a noncontact method of deformation measurement, where the detailed evaluation of strain and strain rate in real time, at specific regions of specimen gauge length can be made.

In this treatment, the yield and post-yield behavior of polycarbonate was assumed to follow the following two distinct paths: an initial viscoelastic path up to a specific deformation that can be accurately defined by the available experimental technique and acts as a control parameter, and a subsequent plastic path that manifests after yielding.

The evaluation of the strain rate in real time plays a decisive role because it can be incorporated into the constitutive equation, leading to the description of stress overshoot. In this way, the strain softening, exhibited by the material response, can be described without any further internal parameters, as is made by various models existing in the literature. Hereafter, only the two parameters N and G_p for the description of strain hardening need to be specified. The observed rate effect of yielding has been depicted with a well-known scaling law.

With this treatment, the exact shape of the experimental stress–strain curve can be illustrated in detail, with only two parameters, as mentioned above. The good approximation between theory and experiment arises from the fact that instead of the typical equations of plasticity widely used in other approaches, a different procedure has been followed here. The separation of deformation into the part that corresponds to the viscoelastic behavior, and that related to the plastic flow, has been made in terms of an earlier treatment, introduced by Rubin. In Rubin's analysis, the inhomogeneous deformation is described by the velocity gradient tensor L, while the elastic F^e and plastic F^p parts of the deformation gradient tensor F need not be defined. The problem that F^e and F^p refer to different configurational states, and are not integrable in the displacement field, is avoided.

REFERENCES

1. Tervoort, T. A.; Klompen, E. T.; Govaert, L. E. J Rheol 1996, 40, 779–797.
2. Ward, I. M. Mechanical Properties of Solid Polymers, 2nd ed.; Wiley: Chichester, UK, 1990.
3. Boyce, M. C.; Parks, M.; Argon, A. S. Mech Mater 1988, 7, 15–33.
4. Wu, P. D.; van der Giessen, E. J Mech Phys Solids 1993, 41, 427–456.
5. Tobolsky, A. V.; Eyring, H. J Chem Phys 1943, 11, 125–134.
6. Haward, R. N.; Thackray, G. Proc London Ser Soc 1968, A302, 453–472.
7. Bernstein, B.; Shokooh, A. J Rheol 1980, 24, 189–211.
8. Matsuoka, S. Relaxation Phenomena in Polymers, 2nd ed.; Hanser Publishers: Munich, 1992; Chap 3.
9. Rubin, M. B. Theory J Solids Struct 1994, 31(19), 2653.
10. Spathis, G.; Kontou, E. Polymer, 1998, 39, 135.
11. G'Sell, C.; Hiver, J. M.; Dahoun, A.; Souahi, A. J Mater Sci 1992, 27, 5031.
12. Bridgman, P. W. Trans Amer Soc Metals 1944, 32, 553.
13. Wolfram, S. Mathematica, A System for Doing Mathematics by Computer, 2nd ed.; Wolfram Research: New York, 1993.
14. Kuhn, W.; Kolloidzeitschrift, F. Grun 1942, 101, 248.
15. Parks, D. M.; Argon, A. S.; Bagepalli, B. MIT Program in Polymer Science and Technology Report; Massachusetts Institute of Technology: Cambridge, MA, 1984.
16. James, H. M.; Guth, E. J Chem Phys 1943, 11, 455.